Constructing Inorganic-Rich Solid Electrolyte Interphase via Adjusting Electrolyte Additives for Stable Li Metal Anodes

Minghui Li[a], Cai Chen[a], Hongze Luo[b], Qingshuai Xu[a], *, Keyou Yan[a], *, Yongcai Qiu[a], * Guangmin Zhou[c]

[a]School of Environment and Energy, State Key Laboratory of Luminescent Materials and Devices, South China University of Technology, Guangzhou, China

[b]Energy Centre, Council for Scientific and Industrial Research (CSIR), P O Box 395, Pretoria, 0001, South Africa.

[c]Tsinghua-Berkeley Shenzhen Institute & Tsinghua Shenzhen International Graduate School, Tsinghua University, Shenzhen, 518055 P. R. China

*Corresponding Author E-mail: 202010108155@mail.scut.edu.cn
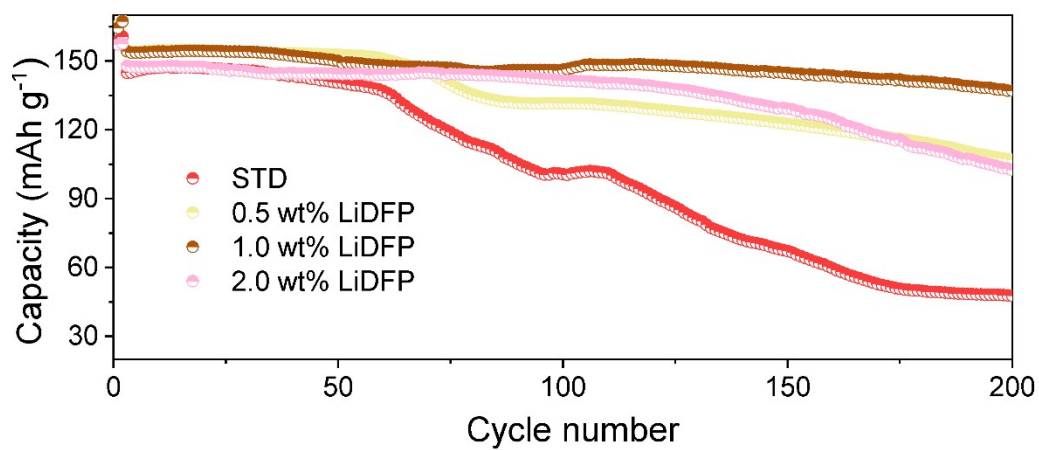
kyyan@scut.edu.cn, ycqiu@scut.edu.cn

Fig. S1. The performance of the Li||LFP full cells in different concentrations (0–2.0 wt%) with LiDFP.
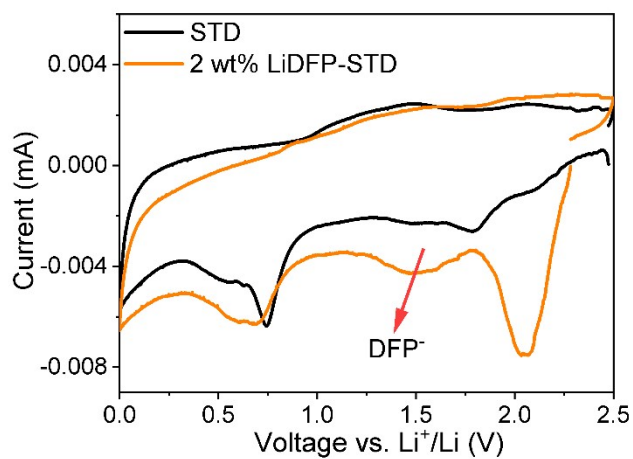
Fig. S2. CV curves of Li∥Cu half cells between a voltage range of 0–2.5 V at a scan rate of 0.2 mV s^{-1}. Comparison of LiDFP reduction peak in LiDFP-STD (orange line) and STD (black line) electrolytes.
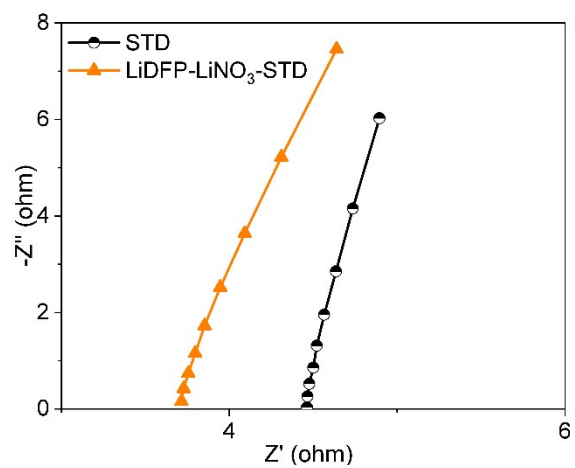
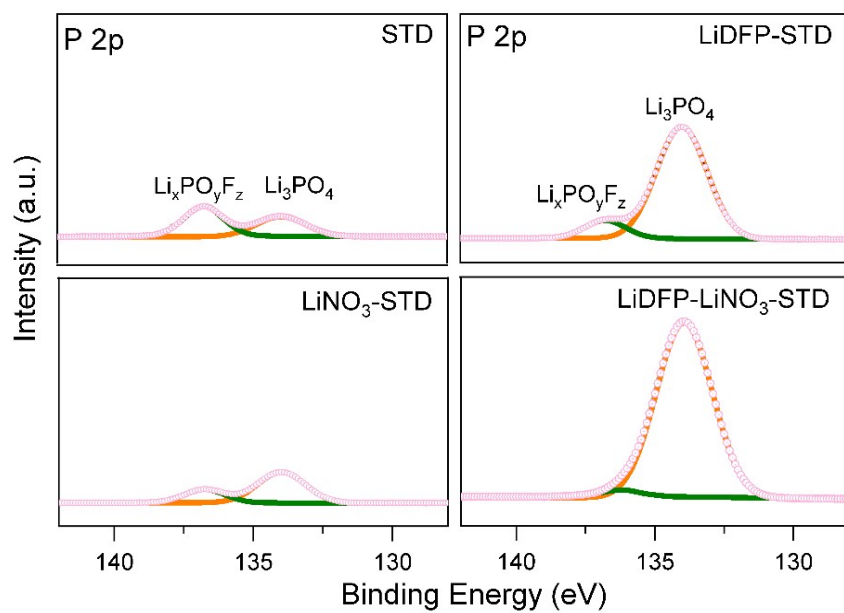Fig. S3. EIS of the SS‖SS symmetric cells with STD and LiDFP-LiNO$_3$-STD.

Fig. S4. P 2p XPS spectra on Li metal surfaces in various electrolytes.
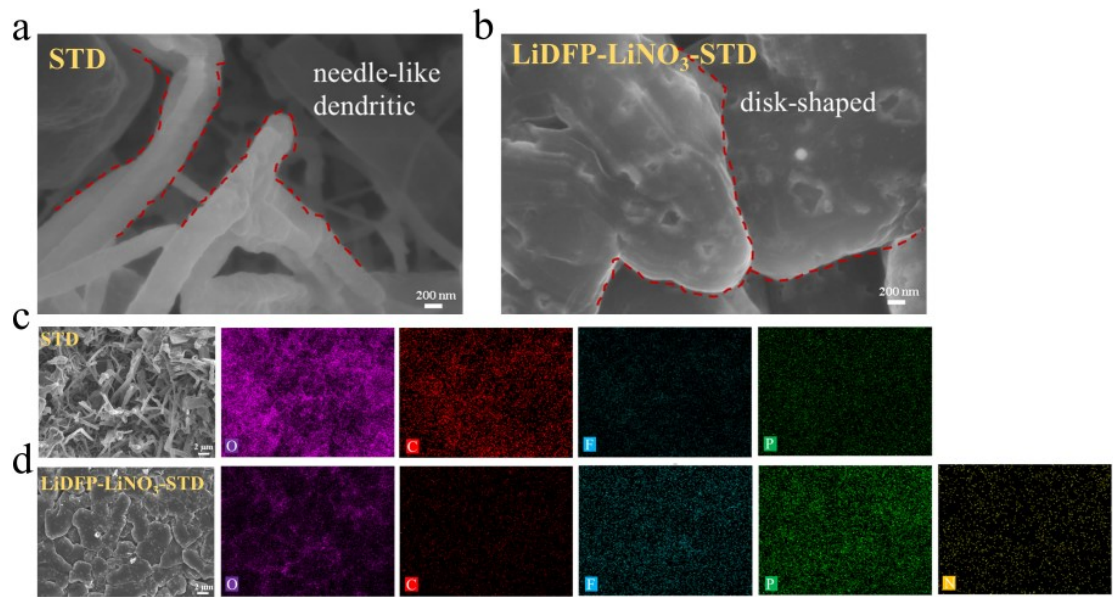
Fig. S5. SEM images of the electrodeposited Li at 0.5 mA cm^{-2} with fixed 5.0 mAh cm^{-2} on Cu foils with (a)STD and (b)LiDFP-LiNO$_3$-STD at 20000x magnification, (c)STD, (d)LiDFP-LiNO$_3$-STD at 3000x magnification and the corresponding mapping images, respectively.
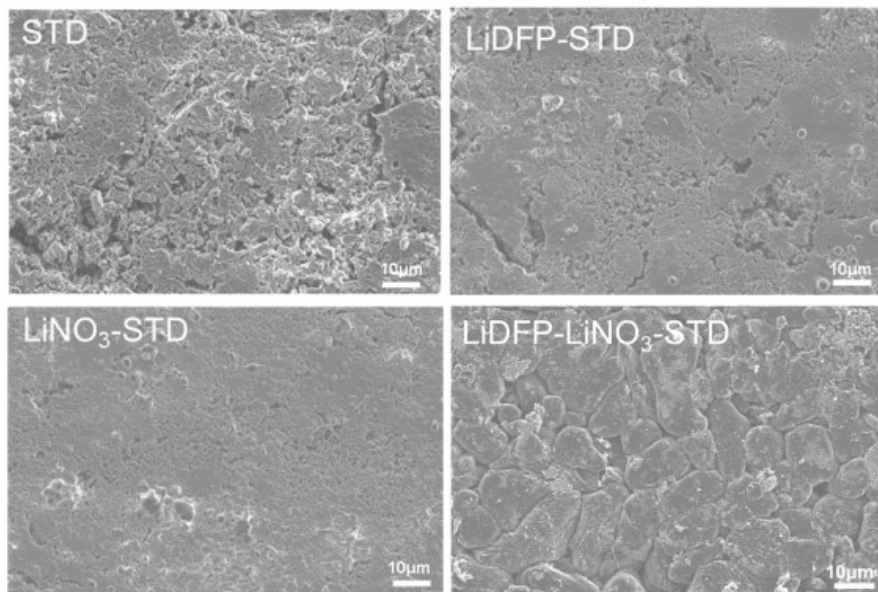
Fig. S6. SEM images top views of the Li metal anode of Li||Li cells after 120 cycles at 1.0 mA cm^{-2} with fixed 1.0 mAh cm^{-2}.
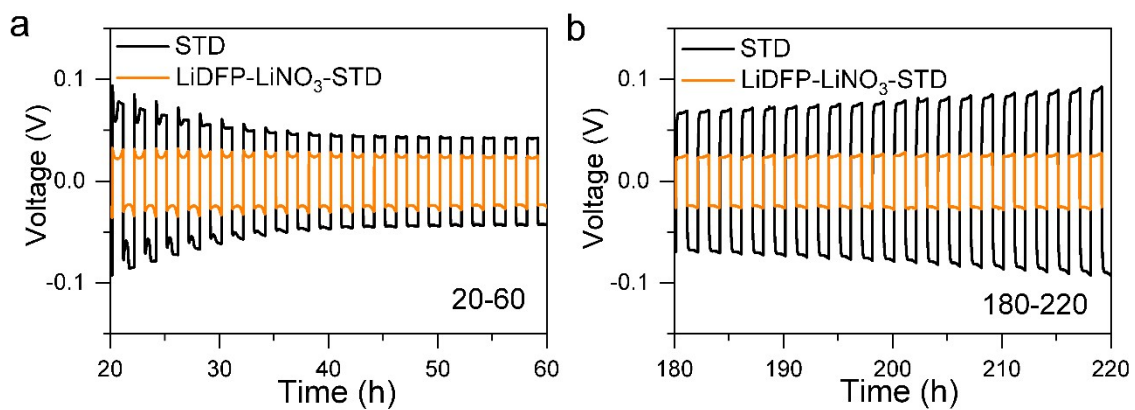
Fig. S7. Detailed analysis of Li‖Li cells voltage profiles at a current density of 1.0 mA cm^{-2} with a capacity of 1.0 mAh cm^{-2} in STD and LiDFP-LiNO$_3$-STD.
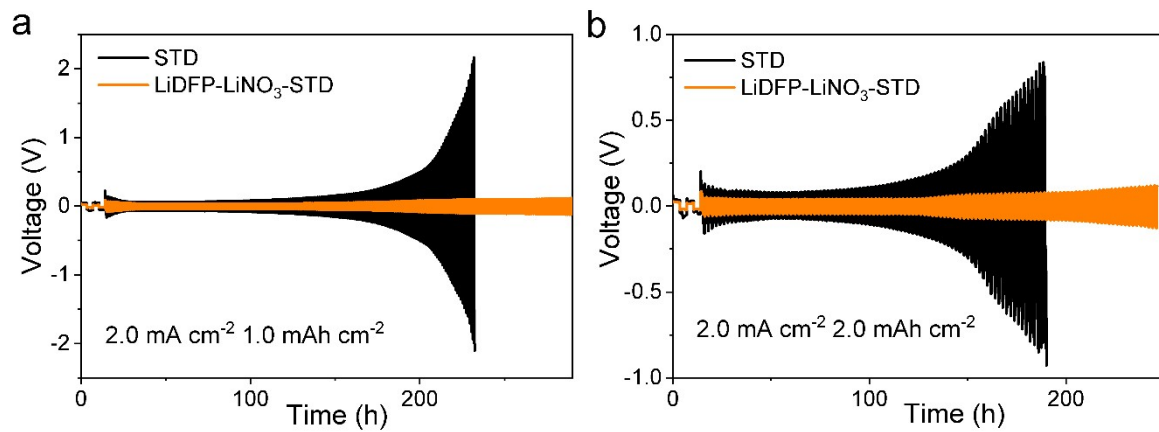
Fig. S8. Cycling performance of the Li∥Li symmetric cells at a current density of 2.0 mA cm^{-2} with a fixed capacity of 1.0 mAh cm^{-2} (a) and a fixed capacity of 2.0 mAh cm^{-2} (b) in various electrolytes.
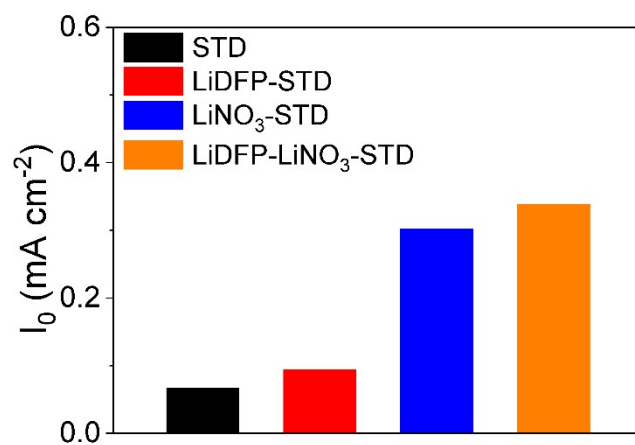
Fig. S9. Exchange current densities (I_0) values fitted of various electrolytes according to Fig. 3d.
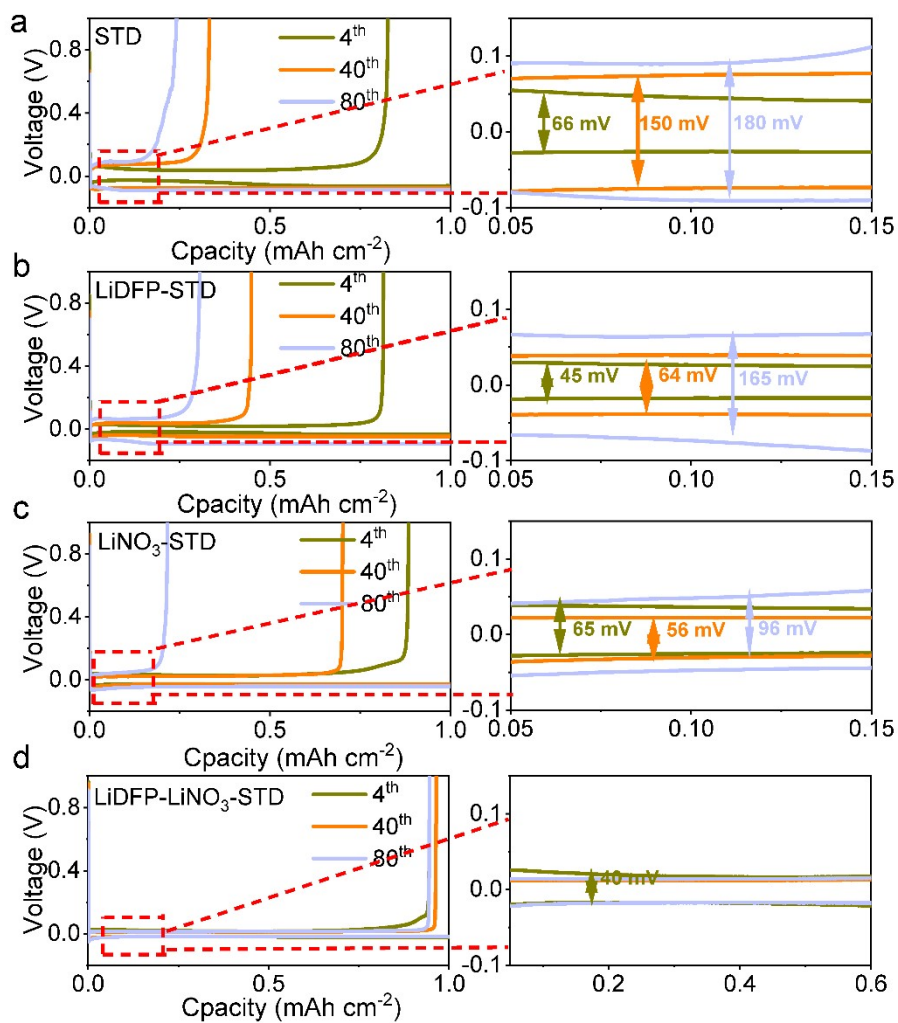
Fig. S10. Li metal deposition/stripping voltage profiles at 4th, 40th, and 80th in various electrolytes.
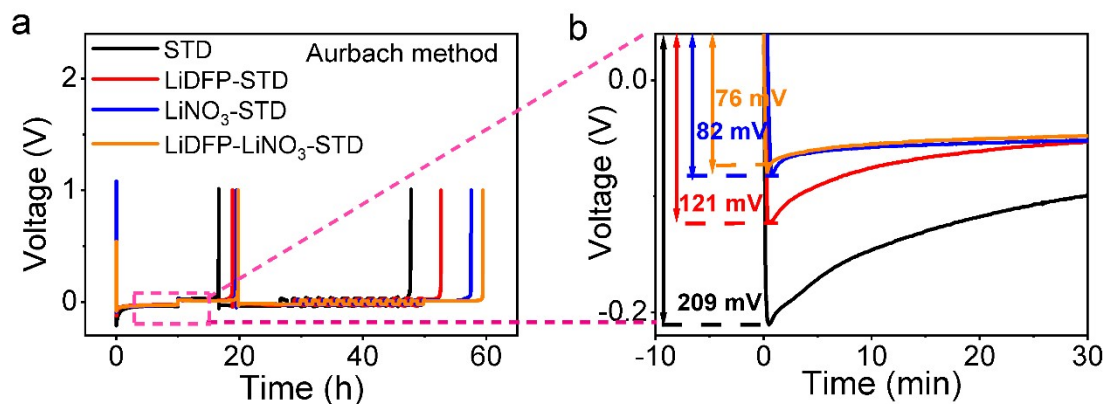
Fig. S11. (a) Coulombic efficiency of Li plating/stripping in different electrolytes by using the Aurbach method. (b) Magnified view of the Li nucleation potential in various electrolytes.
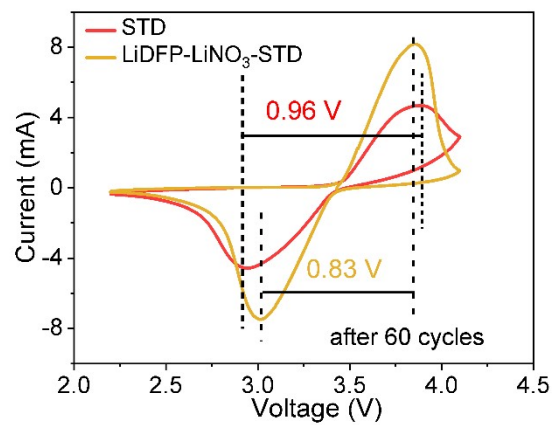
Fig. S12. Cyclic voltammetry of the Li‖LFP cells in the voltage range of 2.2–4.1 V with a scanning speed of 0.2 mV s^{-1}.
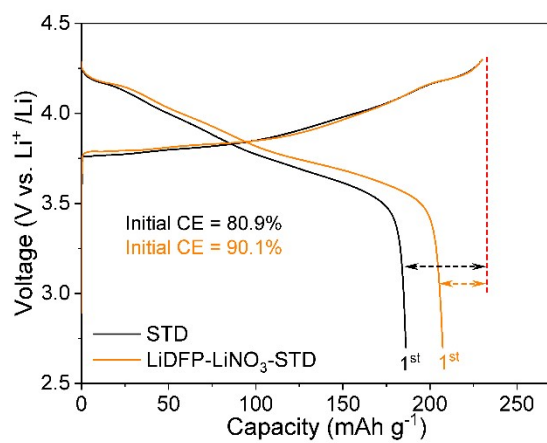
Fig. S13. The first cycle of charge-discharge curve and initial CE values of Li‖NCM811 full cells in different electrolytes.
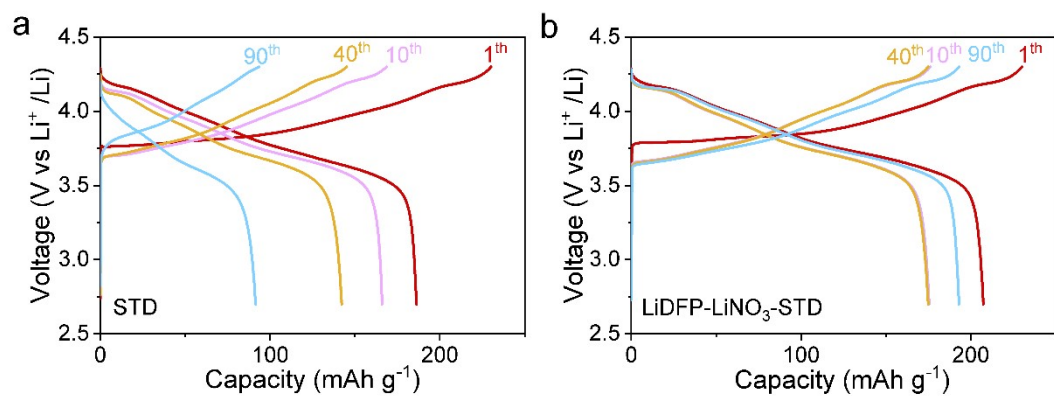
Fig. S14. Charge-discharge profiles of Li‖NCM811 full cells assembled with STD electrolyte (a) and LiDFP-LiNO$_3$-STD-electrolyte (b) at 1th, 10th, 40th, 90th cycle.
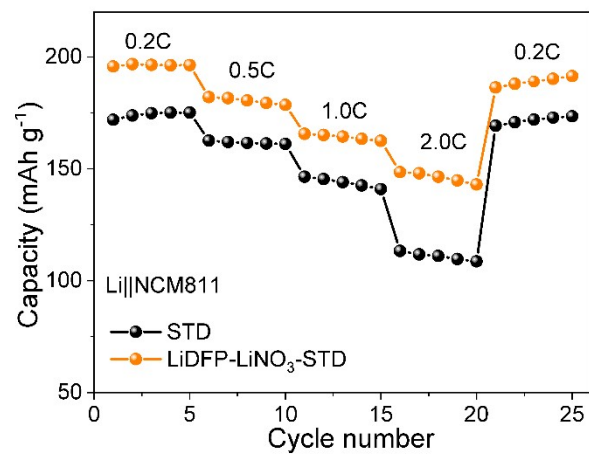
Fig. S15. Rate performance of the Li||NCM811 cells cycled between 2.7–4.3 V at various C-rates from 0.2 C to 2.0 C.